Quantum interference effects in saturated absorption spectroscopy of n=2 triplet-helium fine structure

A. Marsman, M. Horbatsch, and E. A. Hessels

Phys. Rev. A **91**, 062506 — Published 22 June 2015

DOI: 10.1103/PhysRevA.91.062506

Quantum Interference Effects in Saturated Absorption Spectroscopy of n=2 Triplet-Helium Fine Structure

A. Marsman, M. Horbatsch,* and E.A. Hessels
Department of Physics and Astronomy, York University, Toronto, Ontario M3J 1P3, Canada

Over the past decade, precision measurements of the helium $2\,^3P$ fine-structure intervals have been performed using a variety of experimental techniques. We have shown in previous work (Phys. Rev. A 89, 043403, and references therein) that these measurements can be significantly shifted by quantum interference with neighboring transitions, despite the fact that the neighboring transitions are more than a thousand natural widths away from the transition being measured. The shifts depend on the experimental technique used, since different techniques allow for different quantum-mechanical interference paths. Here we consider measurements using the saturated absorption technique, and find that quantum interference effects cause substantial shifts for the $2\,^3P_1$—$2\,^3P_2$ interval. We find that four independent measurements for this interval are now in agreement when interference shifts are taken into account.

PACS numbers: \pacs{32.70.Jz,32.80.-t}

I. INTRODUCTION

Use of the helium $2\,^3P$ triplet intervals to determine the value of the fine-structure constant α has been the focus of ongoing theoretical [1–7] and experimental [8–17] efforts which have yielded increasingly accurate values for these intervals. A determination of α to a part-per-billion or better from a comparison between experimental and theoretical values for the intervals may soon be possible.

At the level of accuracy obtained in these measurements, the effects of off-resonant transitions on the driven resonance become important, despite the fact that these off-resonant transitions are separated from the main resonance by more than a thousand natural widths. Quantum-mechanical interference between the dominant excitation and the off-resonant process induces distortions in the lineshape and results in significant shifts. The scale of these interference shifts depends strongly on the measurement technique, and previous work has demonstrated substantial shifts in laser measurement of the $2\,^3P_1$—$2\,^3P_2$ interval [18], and in saturated-fluorescence spectroscopy of the $2\,^3S_1$—$2\,^3P_1$ and $2\,^3S_1$—$2\,^3P_0$ transitions [19]. Smaller interference shifts are found [20] for microwave measurements of the $2\,^3P$ fine structure.

In this article we turn to an analysis of interference effects on saturated-absorption laser measurements of the $2\,^3P$ fine-structure. Precise measurements of all three intervals have been performed [17] using the saturated-absorption method, so it is crucial to understand the size of the interference effects for these measurements. In this work, we focus on the $2\,^3P_1$—$2\,^3P_2$ fine-structure interval, as measurements of the other $2\,^3P$ intervals are further complicated by shifts due to deflection of the atoms by laser light. The interference shifts calculated in this work are larger than the uncertainty of the saturated-absorption measurement [17].

The saturated-absorption method uses laser excitation in an rf-discharge helium cell, and detects the power of the laser beam after it has passed through the sample. The measurement is performed with and without a second counterpropagating laser beam. In both cases, only the forward-beam power is measured, and the difference in observed absorption for the two cases (i.e., with and without the counterpropagating laser beam) forms the saturated-absorption signal. Because of Doppler shifts, only when the laser is tuned to near resonance do both laser beams communicate to the same atoms, and therefore the saturated-absorption signal has a much narrower line width than the full Doppler-broadened laser resonance.

We calculate first the interference effects for the $2\,^3S_1$,m_J=1—$2\,^3P_1$,m_J=1 ($|1\rangle$—$|2\rangle$ in Fig. 1) saturated-absorption measurement. This measurement is shifted due to interference between this transition and the $2\,^3S_1$,m_J=1—$2\,^3P_2$,m_J=1 ($|1\rangle$—$|3\rangle$ in Fig. 1) transition. The measurement can be modeled using a closed four-level system, since any population that starts in the metastable $|1\rangle$ state can only be excited by a linearly-polarized laser beam to $|2\rangle$ or $|3\rangle$, and these can radiatively decay only to $|1\rangle$ or $|0\rangle$. The $2\,^3\mathrm{S}_1$,$m_J = 0$ state ($|0\rangle$) can be considered to be a dark state because the $2\,^3S_1$,m_J=0—$2\,^3P_1$,m_J=0 transition is electric-dipole-forbidden.

II. DENSITY-MATRIX EQUATIONS

To model the saturated-absorption technique for the measurement performed in [17], we consider a laser with frequency ω=2πf and linear polarization $\hat{z}$ interacting with a cloud of metastable helium atoms. The forward beam and the counterpropagating beam travel in the $+\hat{y}$ and $-\hat{y}$ directions, respectively, and both laser beams have a uniform intensity I_0 over the volume of atoms that contribute to the signal. Each Doppler group within the atomic cloud (with velocity v_y in the direction of the

* marko@yorku.ca

laser-beam) is considered separately, with the full signal obtained by averaging over all Doppler groups. An atom with velocity component v_y sees equal and opposite Doppler shifts $\pm\Delta\omega_D = \pm 2\pi\Delta f_D = \pm\omega v_y/c$ for the two laser beams. The total electric field experienced by a moving atom in the laser beams is $\vec{E}(t) = E(t)\hat{z}$, with

$$E(t) = E_0 \cos\left[(\omega + \Delta\omega_D)t\right] + sE_0 \cos\left[(\omega - \Delta\omega_D)t + \Delta\phi\right]. \quad (1)$$

Here, $E_0 = \sqrt{\frac{2I_0}{\epsilon_0 c}}$, $\Delta\phi$ is the phase difference between the two laser beams, and the parameter $s = 1$ or 0 indicates if the counterpropagating laser beam is switched on or off.

As was done in [21], one can write density-matrix equations describing the transfer of population in the four-level system of Fig. 1, where the population begins in the metastable $|1\rangle$ state, and the laser is nearly resonant with the $|1\rangle$—$|2\rangle$ transition. Since very little population is transferred to the far-off-resonance $|3\rangle$ state, the full set of equations can be approximated [21] by a reduced set of modified density-matrix equations involving only the initial state $|1\rangle$ and the on-resonant state $|2\rangle$:

$$\dot{\rho}_{11} = \left(\frac{i\Omega_2}{2} + \frac{\Omega_3\gamma_{23\to1}}{2\omega_{23}}\right)\rho_{12} + \gamma_{2\to1}\rho_{22} - \left(\frac{i\Omega_2^*}{2} - \frac{\Omega_3^*\gamma_{23\to1}}{2\omega_{23}}\right)\rho_{12}^*, \quad (2a)$$

$$\dot{\rho}_{12} = \frac{i\Omega_2^*}{2}\rho_{11} - \frac{i\Omega_2^*}{2}\rho_{22} - \left[\frac{\gamma_2}{2} + i\left(\Delta_2 + \frac{|\Omega_3|^2}{4\omega_{23}}\right)\right]\rho_{12}, \quad (2b)$$

$$\dot{\rho}_{22} = \frac{i\Omega_2^*}{2}\rho_{12}^* - \frac{i\Omega_2}{2}\rho_{12} - \gamma_2\rho_{22}. \quad (2c)$$

Here ω_{23} is the fine-structure splitting between $|2\rangle$ and $|3\rangle$ (see Fig. 1), while $\Delta_2 = 2\pi\Delta f$ is the detuning of the laser from the $|1\rangle$—$|2\rangle$ transition frequency. The radiative decay terms involve the quantities $\gamma_2 = \gamma$, $\gamma_{2\to1} = \gamma/2$, and $\gamma_{23\to1} = -\gamma/2$, where $\gamma = 1/\tau$ and $\tau = 98$ ns is the lifetime of the $2\,^3P_J$ states.

We are using the rotating-wave approximation, and the Rabi frequencies Ω_2 and Ω_3 associated with the driven transitions between the metastable state $|1\rangle$ and the two excited states $|2\rangle$ and $|3\rangle$ are given by

$$\Omega_i(t) = \Omega_i^{(+)} + s\Omega_i^{(-)}, \quad (3a)$$

$$\Omega_i^{(+)} = e^{i\Delta\omega_D t}\frac{eE_0}{\hbar}\langle 1|z|i\rangle, \quad (3b)$$

$$\Omega_i^{(-)} = e^{-i(\Delta\omega_D t + \Delta\phi)}\frac{eE_0}{\hbar}\langle 1|z|i\rangle. \quad (3c)$$

The (+) and (−) superscripts refer to the forward and counterpropagating beams, and, as in Eq. 1, the value of s indicates whether the counterpropagating beam is switched on or off.

For Eq. 2, the effect of state $|3\rangle$ is small since $\omega_{23} = 2\pi(2291\text{ MHz})$ is more than 1000 times larger than the other frequency scales (γ, Ω_i, and Δ_2, all of which are $\lesssim 1/\tau$). As in [21], a small parameter η is defined as the ratio of these two frequency scales, and ρ_{33} is of order η^2, and can be ignored. The order-η density-matrix elements ρ_{13} and ρ_{23} are eliminated from the full set of equations, to give Eqs. 2(a)-(c), which are complete to first order in η. The order-η terms in Eq. 2 that result from this elimination are: $\frac{|\Omega_3|^2}{4\omega_{23}}$, which is the usual ac-Stark shift of the $|1\rangle$ state, and $\frac{\Omega_3\gamma_{23\to1}}{2\omega_{23}}$, which represent interference effects in the decay pathways.

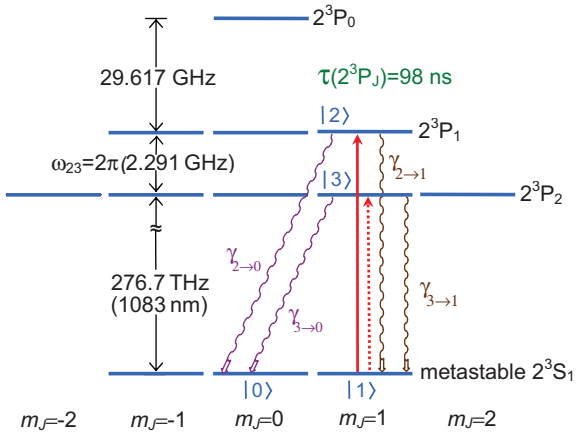

FIG. 1. (Color online) The n=2 triplet energy levels of helium, illustrating the measurement of the $2\,^3S_1, m_J{=}1$—$2\,^3P_1, m_J{=}1$ interval. The population is assumed to start in the $2\,^3S_1, m_J{=}1$ metastable state ($|1\rangle$), and is excited (solid arrow) by a linearly-polarized 1083-nm laser tuned to the $2\,^3P_1, m_J{=}1$ state ($|2\rangle$). There is a small amplitude of also driving (dotted arrow) to the far-off-resonance $2\,^3P_2, m_J{=}1$ state ($|3\rangle$). The atoms can then decay back to $|1\rangle$, or to the $2\,^3S_1, m_J{=}0$ state ($|0\rangle$). The $|0\rangle$ state can be considered to be a dark state due to the electric-dipole-forbidden $2\,^3S_1, m_J{=}0$—$2\,^3P_1, m_J{=}0$ transition, and thus only the four numbered states play a significant role in the measurement.

A. Absorption lineshapes

The saturated-absorption method measures the absorption of the forward laser beam ($\Omega_2^{(+)}$ of Eq. 3(b)). For an atom interacting with the laser for a time T the total absorption is

$$\alpha_s = \frac{i}{2}\int_0^T \left(\Omega_2^{(+)*}\rho_{12}^* - \Omega_2^{(+)}\rho_{12}\right) dt. \quad (4)$$

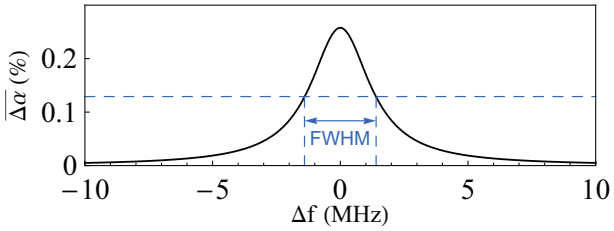

FIG. 2. (Color online) Phase- and Doppler-averaged saturated-absorption lineshape calculated for the $2\,^3S_1$—$2\,^3P_1$ resonance, for a laser intensity of I=0.1 mW/cm^2 and an interaction time of T=1 μs. The points defining the FWHM of the lineshape (in this case 2.8 MHz) are indicated.

This integral, when combined with ρ_{12} obtained by integrating Eq. 2, is complete to order η. All of the integrations are performed numerically, and must be repeated twice: for s=0 and s=1 (i.e., with and without the counterpropagating beam), as indicated by the subscript s in Eq. 4.

The numerical calculation of the difference in absorption $\Delta\alpha$=$\alpha_0 - \alpha_1$ must be repeated for a range of frequencies near resonance to obtain a saturated-absorption lineshape. Such lineshapes must be calculated separately for each Doppler group ($\Delta\omega_D$ of Eq. 1), as well as for each relative phase ($\Delta\phi$ of Eq. 1) and the average, $\overline{\Delta\alpha}$, gives the full lineshape, as shown, for example, in Fig. 2. Since the saturated-absorption lineshape is dominated by atoms that are nearly at rest, it is sufficient to average only over the values of $|\Delta\omega_D|$ <80 MHz.

Figure 3 shows the FWHM of the calculated saturated-absorption lineshape (solid lines) as a function of laser intensity I and of interaction time T (top axis). The feature is broadened both at short interaction times ($T \ll 2\pi\tau$) and above saturation ($\Omega_2 T \gg 1$), but can approach the natural width (dashed line) for sufficiently-long T and low enough I.

Collisions of n=2 helium atoms in the discharge with the much larger number of ground-state atoms in the cell determine the interaction time T. Velocity-changing collisions move atoms to different Doppler groups, and therefore the rate of these collisions determines the time T spent in the Doppler group that contributes to the saturated-absorption signal. Thus, as in [17], an approximate correspondence can be made between the reciprocal of the pressure P in the cell and the interaction time T: $T = C/P$. To find the constant C, we plot measured [22] saturated-absorptions widths (points in Fig. 3) and adjust C (and therefore the bottom axis of Fig. 3) to obtain the best match between the experimental points and our calculated widths for a laser intensity of I=0.1 mW/cm^2.

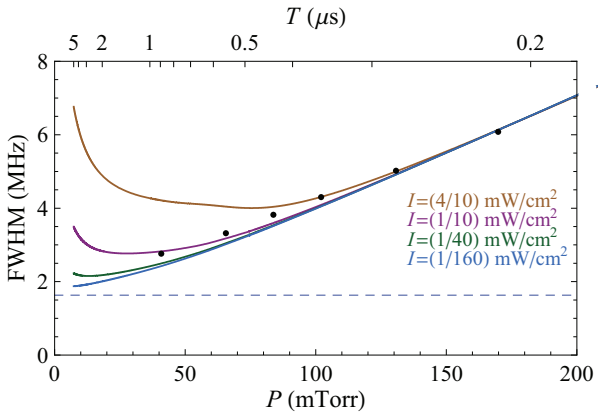

FIG. 3. (Color online) Widths of the calculated saturated-absorption line shapes (solid lines) for the $2\,^3S_1$—$2\,^3P_1$ resonance, over a range of interaction times T, and for various laser intensities, I. The data points are experimental widths [22], which are used to calibrate the pressure scale (bottom axis) with the time scale (top axis). The natural width of the resonance is shown as a dashed line.

III. INTERFERENCE SHIFTS

The quantum-mechanical interference effect that is being considered in this work (which leads to the ω_{23}^{-1} terms in Eq. 2) causes shifted lineshapes. After numerically calculating the saturated-absorption lineshape, the half-maximum points (see Fig. 2) are used to determine the shift. As shown in Fig. 4, the shift depends on how many Doppler groups are included in the calculation, and is fully converged if all Doppler groups with $|\Delta f_D|$<20 MHz are included.

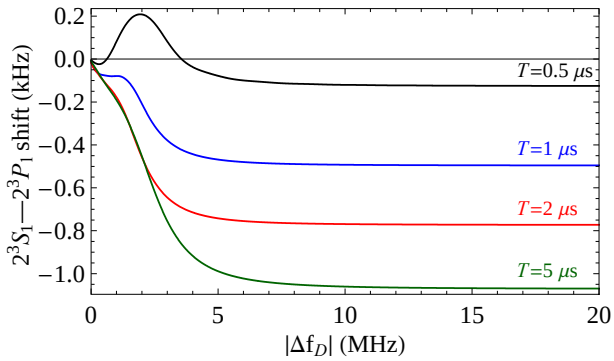

FIG. 4. (Color online) Shifts in the $2\,^3S_1$—$2\,^3P_1$ resonance as a function of included Doppler groups. The shifts are calculated using uniformly-distributed Doppler groups ranging from $-|\Delta f_D|$ to $|\Delta f_D|$. Results are shown for a laser intensity of 0.1 mW/cm^2, with four choices of atom-laser interaction times T. The shift has converged when all Doppler groups with $|\Delta f_D|$<20 MHz are included, and thus the total shift from all Doppler groups is the value at the right of each curve.

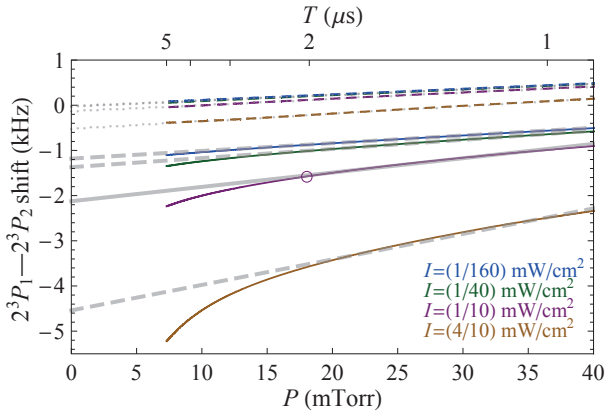

FIG. 5. (Color online) Total shifts (solid thin lines) in the $2\,^3P_1$—$2\,^3P_2$ interval over a range of interaction times T (which result from helium cell pressures P) and laser intensities I. The thin dashed lines give the effect when only the AC shift term is included (and the $\frac{\Omega_3\gamma_{23\to1}}{2\omega_{23}}$ term in Eq. 2 is artificially set to zero) The thick lines show least-squares fits of the shifts over the pressure range of 18 to 38 mTorr, extrapolated to zero pressure. The circle indicates the intensity and pressure at which the most significant data in [17] were taken.

The analysis thus far has been for the $2\,^3S_1$,m_J=1—$2\,^3P_1$,m_J=1 transition. Identical shifts are obtained when considering the m_J=-1 transition. Also, a similar calculation can be carried out for a laser nearly resonant with the $2\,^3S_1$—$2\,^3P_2$ transitions. Every part of the analysis is similar, except for a sign which results from the fact that in this instance the on-resonance process is at a lower (rather than higher) frequency than the off-resonant ($2\,^3S_1$—$2\,^3P_1$) process. A concern that arises when considering the $2\,^3S_1$—$2\,^3P_2$ transition is that more than four states could be involved, since any population that decays to the $2\,^3S_1$,m_J=0 state (state $|0\rangle$ in Fig. 1) could be excited to the $2\,^3P_2$,m_J=0 state. However, as in [17], a sufficiently large magnetic field can remove the degeneracy of the m_J levels, and therefore suppress this transition, leading once again to a four-level system.

In the saturated-absorption measurements in Ref. [17], the $2\,^3P_1$—$2\,^3P_2$ fine-structure interval is determined by subtracting the observed linecenters for the $2\,^3S_1$—$2\,^3P_1$ and $2\,^3S_1$—$2\,^3P_2$ intervals. Because of the equal and opposite shifts, the net shift in the fine-structure interval is two times larger than the shift for the individual transitions, and this shift is shown using solid curves in Fig. 5 for a range of interaction times T and laser intensities I.

For the measurement in [17], the most precise data were taken for helium cell pressures between 18 and 38 mTorr, and were then extrapolated to zero pressure. The thick lines in Fig. 5 show extrapolations of our calculated shifts from this same pressure range. Note that this pressure range avoids the larger interference shifts calculated for lower pressures (larger T) and larger I in Fig. 5, These larger shifts result from the larger line widths (see Fig. 3) for these T and I, which allows for more interference with the neighboring resonance. With the extrapolations to P=0, the interference shifts still remain nonzero. This holds true even in the limit of zero laser intensity I. Thus, a repetition of experiments down to lower and lower pressures and laser intensities will not eliminate the interference shift. As indicated by the lowest-intensity thick dashed line, the interference shift in the limit of zero I and P is −1.2 kHz. This is larger than the 0.51-kHz uncertainty of the saturated-absorption measurement [17] of this interval, and thus it must be carefully considered and corrected for in these measurements.

The thin dashed lines in Fig. 5 show the shifts that result if the $\frac{\Omega_3\gamma_{23\to1}}{2\omega_{23}}$ term in Eq. 2 is artificially suppressed. These dashed curves therefore give only the shifts due to the $\frac{|\Omega_3|^2}{4\omega_{23}}$ term (the ac-Stark shift term). This part of the shift does go to zero in the limit of zero P and I, as indicated by the thick dotted lines, and therefore it is the $\frac{\Omega_3\gamma_{23\to1}}{2\omega_{23}}$ term which leads to the −1.2 kHz shift.

The net −1.2 kHz shift can be broken up into three parts. The shift at 18 mTorr and 0.1 mW/cm^2 (the pressure and intensity at which the most precise data were taken in [17], as indicated by the circle in Fig. 5) is −1.6 kHz. The extrapolation to zero pressure (the thick solid line) causes an additional shift of −0.6 kHz. Finally, an extrapolation of the P=0 intercepts of Fig. 5 to zero intensity causes an additional shift of +1.0 kHz.

The extrapolations of our calculated shifts to P=0 and I=0 are certainly not exact. For example, a helium cell at a pressure P would have a range of times T between velocity-changing collisions (ranging from approximately 50% to 150% of the average T), and therefore the correspondence between T and P assumed in Fig. 5 is only approximate. Furthermore, the current modeling does not explicitly include magnetic fields, and the degree to which state $|0\rangle$ of Fig. 1 is a dark state might depend on magnetic field, on laser intensity, and on the pressure in the cell. Because of such uncertainties, we include a 50% uncertainty for each of the components of the shift and estimate a total shift of $(-1.6 \pm 0.8$ kHz) + $(-0.6 \pm 0.3$ kHz) + $(+1.0 \pm 0.5$ kHz) = -1.2 ± 1.0 kHz for this measurement.

Fig. 6 gives a summary of the current experimental (a - d) and theoretical (e) determinations of the $2\,^3P_1$—$2\,^3P_2$ fine-structure interval. In that figure, the solid error bars are measurements without corrections for interference effects. Each measurement uses a different technique (microwave separated oscillatory fields (a), laser spectroscopy in a laser-cooled beam (b), laser spectroscopy in a well-collimated thermal beam (c), and saturated-absorption spectroscopy in a cell (d), respectively), and therefore each has different interference processes, and requires a separate calculation for the interference shift. The first three of these calculations have been previously completed ([20], [16], and [18]), and the correction for the fourth is considered in this work. The correction is small for the microwave measurement, both because it has a subnatural line width and because the separation

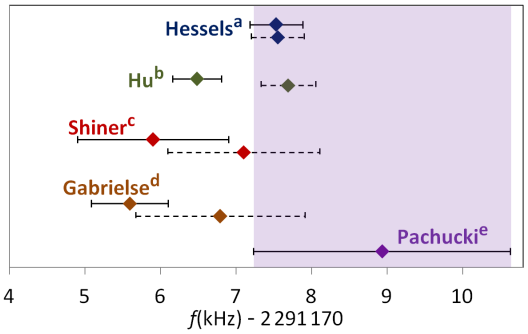

FIG. 6. (Color online) Measurements and theory for the $2\,^3P_1$—$2\,^3P_2$ fine-structure interval in helium. The points labeled a [10], b [16], c [23] and d [17] are measurements, with each using a different experimental technique. The point labeled e is the calculation of Pachucki and Yerokhin [7], adjusted for the CODATA 2010 [24] value of α. The solid error bars are the values without interference effects. The correction for interference effects have now been estimated for all of these measurements (in [20], [16], [18], and in this work, respectively), and the dashed error bars give the corrected measurements.

between the observed resonance and its nearest neighbor is an order of magnitude larger than in the other cases. Even the sign of the shifts depends on the details of the measurement technique (as shown, e.g., in [19]), and thus it is coincidental that the shifts are similar for the other three measurements. The corrected measurements (which include the interference effects and their estimated uncertainties) are shown as dashed error bars in Fig. 6. Note that the corrected values show much better agreement with each other and with theory than the uncorrected values.

IV. CONCLUSIONS

We have calculated the effect of quantum-mechanical interference with a far-off-resonant transition on the saturated-absorption measurements of the $2\,^3P_1$—$2\,^3P_2$ fine-structure interval in atomic helium. The effect is found to cause a shift that is large compared to the measurement uncertainty, and therefore must be properly accounted for. The shift is significant even though the off-resonant transition is separated by 2.3 GHz, or 1400 natural widths. This work illustrates that shifts due to quantum-mechanical interference must be carefully considered for all precision measurements. When possible, measurements should be planned to minimize the interference effect (as, for example, for point a of Fig. 6), by either ensuring that the separation between resonances is very large, or by techniques which suppress any nonresonant processes. To correct for the interference shifts, a calculation must be performed based on the exact measurement technique used.

V. ACKNOWLEDGEMENTS

This work is supported by NSERC, CRC and NIST, with computations done using SHARCNET.

[1] Z.-C. Yan and G. W. F. Drake, Phys. Rev. Lett. **74**, 4791 (1995).
[2] T. Zhang, Z.-C. Yan, and G. W. F. Drake, Phys. Rev. Lett. **77**, 1715 (1996).
[3] G. W. F. Drake, Can. J. Phys. **80**, 1195 (2002).
[4] K. Pachucki and J. Sapirstein, J. Phys. B **33**, 5297 (2000).
[5] K. Pachucki and J. Sapirstein, J. Phys. B **36**, 803 (2003).
[6] K. Pachucki, Phys. Rev. Lett. **97**, 013002 (2006).
[7] K. Pachucki and V. A. Yerokhin, Phys. Rev. Lett. **104**, 070403 (2010).
[8] C. H. Storry, M. C. George, and E. A. Hessels, Phys. Rev. Lett. **84**, 3274 (2000).
[9] M. C. George, L. D. Lombardi, and E. A. Hessels, Phys. Rev. Lett. **87**, 173002 (2001).
[10] J. S. Borbely, M. C. George, L. D. Lombardi, M. Weel, D. W. Fitzakerley, and E. A. Hessels, Phys. Rev. A **79**, 060503 (2009).
[11] F. Minardi, G. Bianchini, P. C. Pastor, G. Giusfredi, F. S. Pavone, and M. Inguscio, Phys. Rev. Lett. **82**, 1112 (1999).
[12] P. C. Pastor, G. Giusfredi, P. DeNatale, G. Hagel, C. de Mauro, and M. Inguscio, Phys. Rev. Lett. **92**, 023001 (2004).
[13] D. Shiner, R. Dixson, and P. Zhao, Phys. Rev. Lett. **72**, 1802 (1994).
[14] M. Smiciklas and D. Shiner, Phys. Rev. Lett. **105**, 123001 (2010).
[15] C. H. Storry and E. A. Hessels, Phys. Rev. A **58**, R8 (1998).
[16] G.-P. Feng, X. Zheng, Y. R. Sun, and S.-M. Hu, Phys. Rev. A **91**, 030502 (2015).
[17] T. Zelevinsky, D. Farkas, and G. Gabrielse, Phys. Rev. Lett. **95**, 203001 (2005).
[18] A. Marsman, M. Horbatsch, and E. A. Hessels, Phys. Rev. A **86**, 040501 (2012).
[19] A. Marsman, E. A. Hessels, and M. Horbatsch, Phys. Rev. A **89**, 043403 (2014).
[20] A. Marsman, M. Horbatsch, and E. A. Hessels, Phys. Rev. A **86**, 012510 (2012).
[21] M. Horbatsch and E. A. Hessels, Phys. Rev. A **84**, 032508 (2011).
[22] T. Zelevinsky, *Helium 2^3P Fine Structure Measurement in a Disharge Cell; Thesis (supervisor: G. Gabrielse), Harvard University* (2004).
[23] J. Castillega, D. Livingston, A. Sanders, and D. Shiner, Phys. Rev. Lett. **84**, 4321 (2000).
[24] P. J. Mohr, B. N. Taylor, and D. B. Newell, J. Phys. Chem. Ref. Data **41**, 043109 (2012).